

Use of a multiwavelength pyrometer in several elevated temperature aerospace applications

Daniel Ng^{a)} and Gustave Fralick
NASA Glenn Research Center, Cleveland, Ohio 44135

(Received 27 April 2000; accepted for publication 20 November 2000)

A multiwavelength pyrometer was developed for applications unique to aerospace environments. It was shown to be a useful and versatile technique for measuring temperature, even when the emissivity is unknown. It has also been used to measure the surface temperatures of ceramic zirconia thermal barrier coatings and alumina. The close agreement between pyrometer and thin film thermocouple temperatures provided an independent check. Other applications of the multiwavelength pyrometer are simultaneous surface and bulk temperature measurements of a transparent material, and combustion gas temperature measurement using a special probe interfaced to the multiwavelength pyrometer via an optical fiber. The multiwavelength pyrometer determined temperature by transforming the radiation spectrum in a broad wavelength region to produce a straight line (in a certain spectral region), whose intercept in the vertical axis gives the temperature. Implicit in a two-color pyrometer is the assumption of wavelength independent emissivity. Though the two data points of a two-color pyrometer similarly processed would result immediately in a similar straight line to give the unknown temperature, the two-color pyrometer lacks the greater data redundancy of the multiwavelength pyrometer, which enables it to do so with improved accuracy. It also confirms that emissivity is indeed wavelength independent, as evidenced by a multitude of the data lying on a simple straight line. The multiwavelength pyrometer was also used to study the optical transmission properties of a nanostructured material from which a quadratic exponential functional frequency dependence of its spectral transmission was determined. Finally, by operating the multiwavelength pyrometer in a very wide field of view mode, the surface temperature distribution of a large hot surface was obtained through measurement of just a single radiation spectrum. [DOI: 10.1063/1.1340558]

I. INTRODUCTION

Often in aerospace application, measurements of surface temperature using the traditional one-color pyrometers suffer from the requirements of having to know the emissivity of the measured surface and the transmissivity of the intervening optical medium. With the assumption that the emissivity is independent of the two colors (wavelengths), two-color ratio pyrometers do not need to know the emissivity. For many newly developed and special materials, emissivity and information that emissivity is wavelength independent is unavailable or difficult to obtain before attempting a temperature measurement. Often, whatever information is available is of limited precision and unknown certainty. In particular, a two-color pyrometer is unable to ascertain whether the material's emissivity is indeed independent of wavelength. The multiwavelength pyrometer was developed to address these surface temperature measurement limitations. It provides confirmation of the assumption that a material's emissivity is spectrally independent, enhancing confidence in temperature measurement. We describe here briefly its development and some successful applications.

II. EXPERIMENT

A. Pyrometer spectrometer

Pyrometry and multiwavelength pyrometry¹⁻⁵ are remote temperature measurement techniques. A multiwavelength pyrometer basically consists of a spectrometer and a computer. It uses a spectrometer to acquire radiation information over a very wide spectral region. The spectrometer we used is shown schematically in Fig. 1. It is an off-the-shelf commercial⁶ spectral radiometer capable of operating in the spectral range of from 0.5 to 14.5 μm . This spectrometer monochromatizes the radiation using variable circular filters. Other spectrometers and radiation monochromatization techniques could have been used without affecting the measurements. Depending on the temperature measurement requirements, the spectrometer's range of operation was from 0.5 to 2.5, 1.3 to 4.5, or 1.5 to 14.5 μm . Data acquisition, data analysis, and interfacing of data into spreadsheet, graphing, or word processing software are automated.

The spectrometer detects radiation in the respective operation ranges employing combination pair detectors. These detector combinations can be silicon/lead sulfide (Si/PbS), or indium antimonide/mercury cadmium telluride (InSb/MCT). Radiation in the detection ranges is monochromatized into more than 400 channels. Spectrometer signal acquisition is accomplished by a 3 m focal length, 150 mm diameter para-

^{a)}Electronic mail: daniel.l.ng@grc.nasa.gov

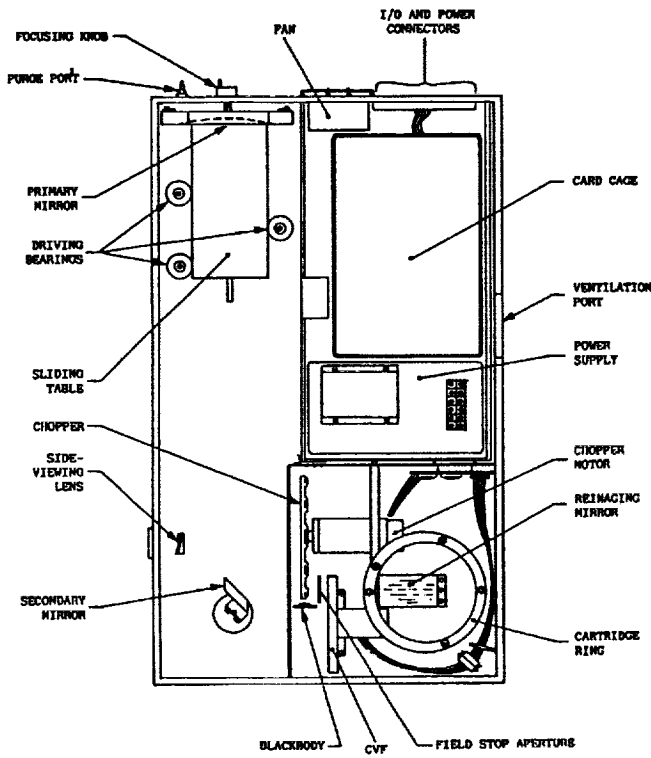


FIG. 1. Schematics of a commercial spectral radiometer.

bolic mirror. As received, this spectrometer requires a minimum distance of 3 m between the spectrometer and target for proper focusing. However, by interfacing the spectrometer with optical fiber signal input, this stringent 3 m requirement is removed. Targets can now be very close up or as far away as 20 m, through the use of a low loss silica fiber to transmit short wavelength radiation acquired in high temperature (>1273 K) measurement applications. Because data acquisition into the spectrometer channels is sequential, the response time of the instrument is slow. To overcome this shortcoming, we plan to replace our spectrometer with a very fast one which will use array detectors and diffraction grating monochromatation.

B. Method

The multiwavelength pyrometer is calibrated with radiation from a black body furnace at a known temperature viewed either through its mirror optics or through the optical fiber interface. The calibration process determines the instrument constants necessary for converting the detector output into radiation intensity at each of the wavelength channels. The emitted radiation (followed by transmission through air or an optical fiber) is described by Planck's law of black body radiation¹

$$L_{\lambda} = \epsilon_{\lambda} \tau_{\lambda} \frac{c_1}{\lambda^5} \frac{1}{\exp(c_2/\lambda T) - 1}$$

$$= \epsilon_{\lambda} \tau_{\lambda} \frac{c_1}{\lambda^5} \exp(-c_2/\lambda T) \frac{1}{1 - \exp(-c_2/\lambda T)}, \quad (1)$$

where $c_1 = 2\pi hc^2$, $c_2 = hc/k$ are the radiation constants, with c being the velocity of light, h Planck's constant, k

Boltzmann's constant, L_{λ} the radiation intensity, ϵ_{λ} the emissivity of the radiation source, and τ_{λ} the transmissivity of the optical medium between the pyrometer and the radiation source at wavelength λ .

For data analysis, Eq. (1) is rewritten as

$$y = \left(\frac{\ln\left(\frac{c_1}{\lambda^5} \frac{1}{L_{\lambda}}\right)}{c_2/\lambda} \right) - \frac{\ln\left(1 - \exp\left(-\frac{c_2}{\lambda T}\right)\right)}{c_2/\lambda}$$

$$= \frac{1}{T} - \frac{\lambda}{c_2} \ln(\epsilon_{\lambda} \tau_{\lambda}). \quad (2)$$

This is the working equation of the traditional one-color pyrometry, which requires knowing the emissivity and or transmissivity. For the multiwavelength pyrometer, neither quantity is required to determine temperature. Because the quantity $(1 - \exp(-c_2/\lambda T))$ is practically unity at short wavelengths (generally a very good approximation), its logarithm is zero. Although in all our experimental data, there is no observable difference between the quantities $[\ln(c_1/(\lambda^5 L_{\lambda}))]/(c_2/\lambda) - \ln(-\exp(-c_2/\lambda T))/(c_2/\lambda)$ and $\ln(c_1/(\lambda^5 L_{\lambda}))]/(c_2/\lambda)$, the authors have learned that for improved accuracy, any errors arising from these differences ought to be addressed, such as by incorporating the work of Levendis *et al.*⁷ While we have not yet incorporated the latter's work into our algorithm, we have taken the corrective term $\ln(1 - \exp(-c_2/\lambda T))/(c_2/\lambda)$ into account iteratively.

Observe from Eq. (2) that if $\ln(\epsilon_{\lambda} \tau_{\lambda})$ is wavelength independent over some wavelength region, plotting either of the quantities $[\ln(c_1/(\lambda^5 L_{\lambda}))]/(c_2/\lambda) - \ln(1 - \exp(-c_2/\lambda T))/(c_2/\lambda)$ or $\ln(c_1/(\lambda^5 L_{\lambda}))]/(c_2/\lambda)$ as a function of λ results in a straight line whose slope is $\ln(\epsilon_{\lambda} \tau_{\lambda})/c_2$. This is the self verifying feature of the multiwavelength pyrometer, confirming that in this spectral region, the emissivity is independent of wavelength. The quantity $1/y$ at each wavelength λ is often referred to as the radiant temperature. By fitting a best straight line to the quantity y derived from experimental data, the inverse of the desired unknown temperature T is determined from the zero wavelength intercept of the fitted line. In all the materials we have studied, even when the emissivity possessed variation over large spectral regions, there always existed a region or regions in which the emissivity was fairly constant or exhibited only such slight variations that the method was applicable. The implicit assumption of the multiwavelength pyrometer that emissivity is independent of wavelength is also assumed by a two-color pyrometer. But a two-color pyrometer is not able to provide verification that this assumption is satisfied, and it also lacks the greater data redundancy, which the multiwavelength pyrometer possesses to provide increased accuracy, confidence, and significance.

III. APPLICATIONS AND RESULTS

The multiwavelength pyrometer has been used in applications ranging from traditional pyrometric temperature measurement of surfaces to many novel applications, such as measuring the temperature of transparent substances, the

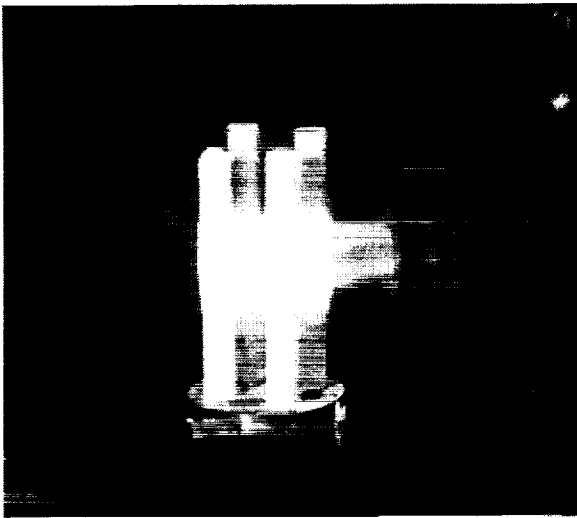


FIG. 2. Experimental arrangement to measure the surface temperature of ZrO_2 surface. The multiwavelength pyrometer is positioned in a roughly perpendicular direction to the ZrO_2 coating surface and the 0.3 Mach atmospheric burner.

temperature of combustion gases, the temperature distribution of a hot surface, and to study the optical properties of nanostructured materials. The results of these applications are described below.

A. Zirconia (ZrO_2) thermal barrier coating (TBC)

Zirconia is a ceramic material widely used as thermal protective coating on turbine engine components to enable them to survive high temperature operation in order to achieve high efficiency and performance. The emissivity of zirconia is generally not well known, and has been observed to vary with time and temperature history.⁸ In this experiment, a 0.3 Mach atmospheric jet burner (Fig. 2) heated the zirconia TBC surface. The mirror optics of the multiwavelength pyrometer were focused on the surface to acquire the spectrum in Fig. 3. The spectrum spanned the spectral region from 1.5 to 4.5 μm . It was analyzed according to Eq. (2) and the result is shown in Fig. 4. The emissivity of zirconia over most of this spectral region is very nearly constant (a fact not previously known), resulting in a very good straight line fit. From the graph's intercept, the temperature of the surface is determined to be 1400 K.

B. Thin film thermocouples on alumina

In this experiment, pyrometrically measured temperatures were compared to those obtained from another temperature measurement technique. In order to measure temperature simultaneously with that using the multiwavelength pyrometer, a type R platinum thin film thermocouple (TFTC) was sputter deposited on the surface of a ceramic alumina substrate. The TFTC was calibrated by equilibrating it in a black body furnace at several known temperatures. This black body furnace also calibrated the multiwavelength pyrometer as described above. The multiwavelength pyrometer was focused on a spot containing the junction of the TFTC. At a field of view (FOV) of 1 mR at 3 m distance, the detection spot was 3 mm in diameter, which was larger than

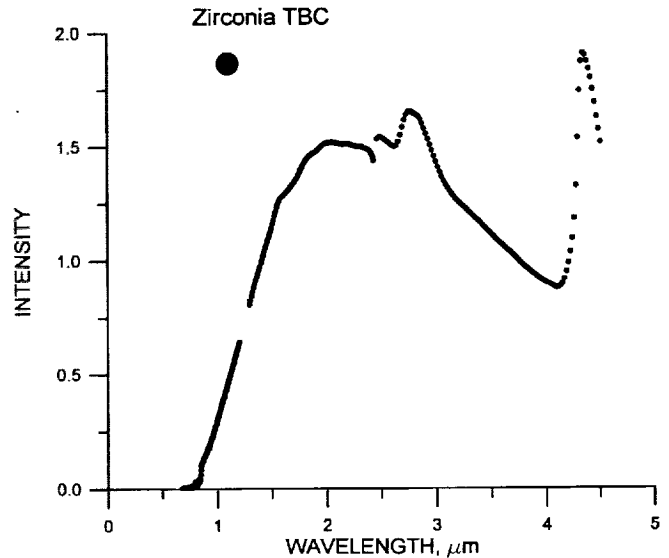


FIG. 3. The radiation spectrum of the heated Zirconia TBC surface.

the TFTC junction. In Fig. 5, an impinging flame heated the alumina substrate on its surface. The TFTC soon indicated a steady temperature. The recorded spectrum (Fig. 6) was analyzed according to Eq. (2) (results shown in Fig. 7) to determine the temperature (1369 K). The pyrometer measured temperature agreed well with the TFTC temperature of 1350 K. If it is desired, one can also determine the surface emissivity from the slope of the fitted straight line and the experimental geometry.

C. Glass material

The analysis of a transparent material is different from that of an opaque material. In general (referring to Fig. 8), the contribution dL_λ to radiation intensity at wavelength λ , emitted from a slab of transparent material, thickness dx , at a distance x from the surface, detected by the pyrometer outside a transparent material is given by⁹

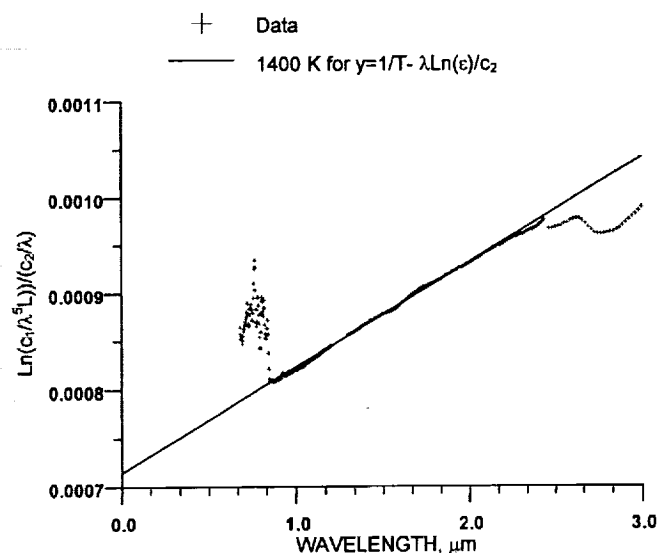


FIG. 4. Plot of the transformed zirconia TBC radiation spectrum.

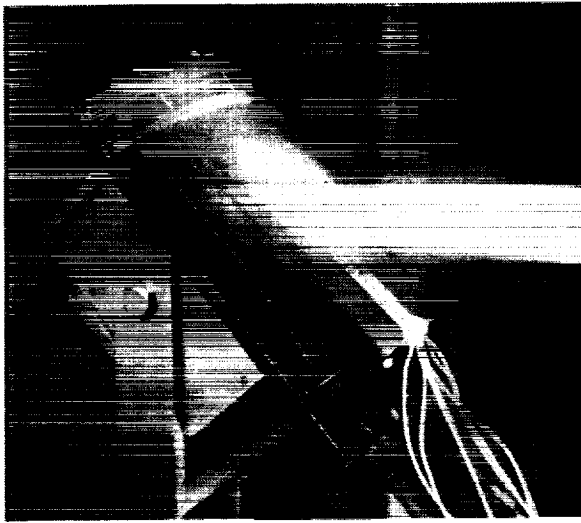


FIG. 5. Experiment done to compare the temperatures of a substrate measured using TFTC and the multiwavelength pyrometer. The multiwavelength pyrometer views the arrangement from a roughly perpendicular direction.

$$dL_\lambda = (1 - R)a \exp(-ax) \frac{c_1}{\lambda^5} \frac{1}{\exp(c_2/\lambda T(x)) - 1} dx, \quad (3)$$

where a is the absorption coefficient of the transparent material, and $T(x)$ is the temperature at x . R is the fraction of radiation that is reflected back into the medium at the interface. Therefore $1 - R$ is the fraction that escapes being reflected. For simplicity, any spectral dependence of R is omitted from the notation. The total contribution from all the slabs from $x=0$ to $x=D$, is obtained by integrating Eq. (3) over this length

$$L_\lambda = (1 - R) \int_0^D a \exp(-ax) \frac{c_1}{\lambda^5} \frac{1}{\exp(c_2/\lambda T(x)) - 1} dx, \quad (4)$$

where D is the total thickness of the transparent medium. The basic experimental geometry used in experiments (A) and (B) was again used for this experiment of a piece of

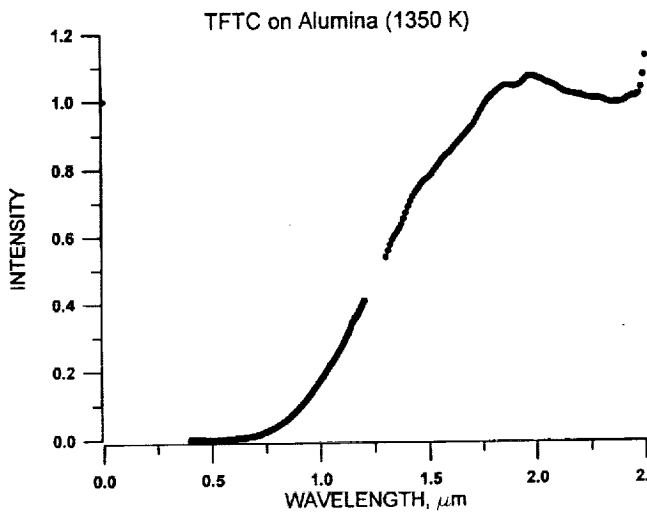


FIG. 6. The radiation spectrum of the TFTC surface.

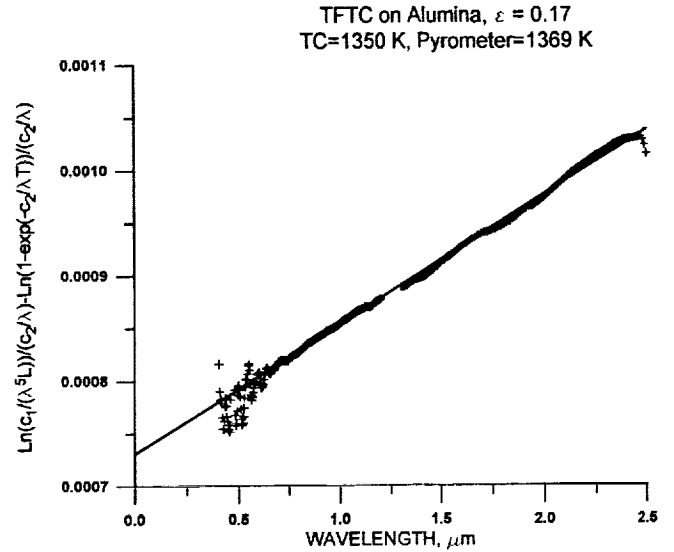


FIG. 7. Plot of the transformed radiation spectrum from the TFTC surface.

glass heated by a propane torch. The spectrum (Fig. 9) of a piece of glass raised in temperature by a propane torch was recorded by the multiwavelength pyrometer. Most of the radiant energy in the spectrum was contained in the spectral region longer than $1 \mu\text{m}$. Equation (2) applies well in this region, as shown by a Planck curve of temperature 1194 K and a value of 0.74 for the term $\text{Ln}(\epsilon_\lambda \tau_\lambda)$ to fit the data. The agreement is extremely good. The deviation near $2.4 \mu\text{m}$ was due to the poor signal to noise in that region. We concluded that a predominant portion of the radiation is surface emission at wavelengths longer than $1 \mu\text{m}$.

In the short wavelength region, the radiation originated from inside the transparent material. In general, there will be a temperature profile $T(x)$ which is a function of x . However, assuming that a characteristic interior temperature T_i can be defined, Eq. (4) is rewritten as

$$L_\lambda = (1 - R) \frac{c_1}{\lambda^5} \exp(-c_2/\lambda T_i) \times \int_0^D a \exp(-ax) \frac{\exp(c_2/\lambda T_i)}{\exp(c_2/\lambda T(x)) - 1} dx \quad (5)$$

for $\exp(c_2/\lambda T_i) \gg 1$, Eq. (5) is simplified to

$$L_\lambda = (c_1/\lambda^5) \exp(-c_2/\lambda T_i) I(T_i, \lambda), \quad (6)$$

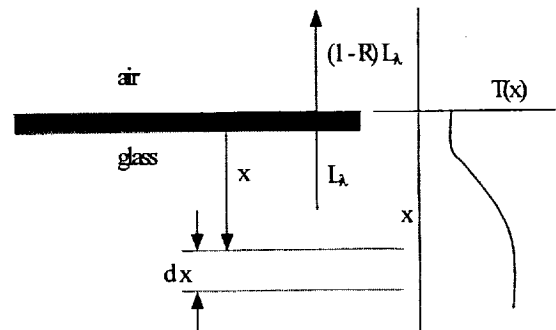


FIG. 8. Schematic depicting radiation emitted from inside a transparent medium.

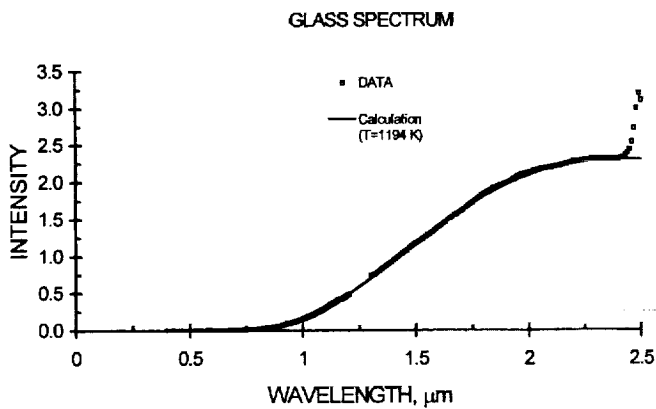


FIG. 9. Radiation spectrum of transparent glass.

where

$$I(T_i, \lambda) = \int_0^D (1-R)a \exp\left(-ax + \frac{c_2}{\lambda} \left(\frac{1}{T_i} + \frac{1}{T(x)}\right)\right) dx. \quad (7)$$

By transforming Eq. (6) according to Eq. (2) into inverse radiant temperatures, we obtain

$$y = \left(\frac{\text{Ln}\left(\frac{c_1}{\lambda^5 L_\lambda}\right)}{\frac{c_2}{\lambda}} \right) = \frac{1}{T_i} - \frac{\lambda}{c_2} \text{Ln}(I(T_i, \lambda)). \quad (8)$$

If $I(T_i, \lambda)$ is independent of λ , a plot of the quantity on the left vs λ will give a straight line, with the intercept equal to the reciprocal of the temperature T_i . The extent to which this assumption is true will be determined by how well the data of the experiment agrees with this interpretation.

The results of analyzing a glass radiation spectrum are shown in Fig. 10. The transformation clearly shows that there are two regions, corresponding to the long and short wavelengths. In the long wavelength region, the radiation comes from the surface. According to Eq. (2), its temperature was 1194 K. The data corresponding to the short wavelength data fell on another straight line segment, implying that the integral defined by Eq. (7) is indeed independent of wavelength. The intercept of this line yielded a bulk temperature of 1136 K. This is 60 K cooler than the surface where the heating took place. The multiwavelength pyrometer measured bulk temperature in the transparent interior as well as the surface temperature.

D. Combustor gas temperature measurement

Turbo machinery combustor exhaust gas has very high temperatures, which can be over 2300 K, easily exceeding the working temperatures of platinum thermocouple materials. The combustor we used in this experiment was an atmospheric burner similar to the one shown in Fig. 2, both in design and in application geometry. Higher temperature thermocouple materials such as tungsten and rhenium exist, but are oxidized easily in the environment of the hot gases. A combustion gas temperature probe (Fig. 11) was designed at the National Aeronautics Space Administration (NASA).¹⁰ Tungsten/rhenium thermocouples measured the internal temperature of a protective tubular beryllia shroud, which was

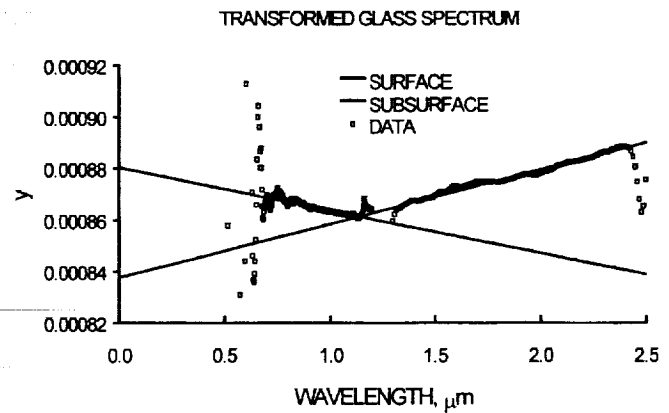


FIG. 10. Plot of transformed radiation spectrum from transparent glass illustrating the behaviors of internal and surface radiations.

inserted into the path of the exhausting combustion gases. The combustion gas temperature was inferred from a heat transfer modeling calculation using the thermocouple temperature. Though beryllia can operate to at least 2670 K, an inert (argon) atmosphere was necessary inside the shroud tubing to prevent tungsten and rhenium metal oxidation. Enhanced performance of this combustion gas temperature measurement probe was achieved by dispensing with the thermocouple and by instead incorporating the multiwavelength pyrometer. Radiation from the internal beryllia probe wall was coupled by fiber optics to the multiwavelength pyrometer to measure the beryllia temperature and hence the combustion gas temperature. The usual calibration using a black body was performed ahead of time. The apertured low loss silica fiber was positioned at the cold end of the protective probe. Its incorporation eliminated the necessity for inert gas which the use of tungsten and rhenium thermocouples required. The fiber optics data of the probe acquired in the atmospheric burner operating at two levels were transformed as before and shown in Figs. 12 and 13. The temperatures of the gas temperature probe were determined to be 1360 and 1745 K, respectively. The precipitous decrease in signal above 2 μm was due to the silica fiber transmission loss in that region. The only means of comparison was a type S thermocouple inserted into the flame at the burner lip, reading 1300 and 1580 K, respectively. To avoid being destroyed by the hot gases in the central flow of the burner, the thermocouples were positioned at the cooler periphery of the flame. The probe was therefore measuring the hottest region of the flame at the center. Wavelength 1.3 μm is near the region where the spectrometer switches from one detector to another. Neither detector is very sensitive here. The rather bad data appearing in Figs. 12 and 13 near this region was



FIG. 11. BeO combustion gas temperature probe.

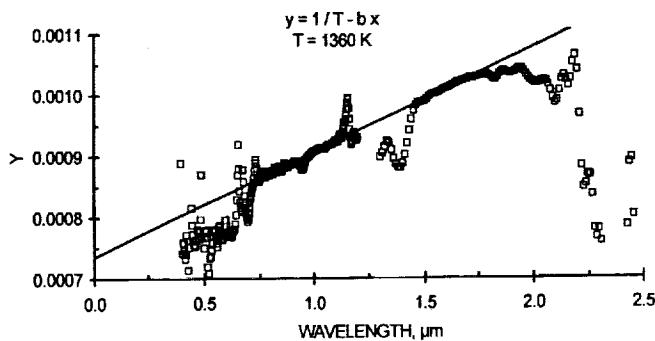


FIG. 12. Plot of the transformed radiation spectrum from a BeO gas temperature probe at 1360 K.

the result of a combination of degrading sensor spectral detectivity and higher absorption by the high OH silica fiber occurring there.

E. Nanostructured thermal barrier coating

Experiments to record the spectra of (i) a black body furnace, (ii) its transmission intensity through a plain sapphire disk, and (iii) its transmission intensity through a sapphire disk having a nanostructured coating deposited on it were performed as shown in Fig. 14. These spectra are shown in Fig. 15. The transmission coefficients τ of the plain sapphire disk (obtained from dividing the sapphire transmission by the black body intensity) and that of the coated sapphire disk are shown in Fig. 16. Nanostructured coating is a proprietary substance. Its exact structure, chemical composition, and manufacture process are guarded and not revealed by the manufacturer. It is only known that its total thickness is about $25 \mu\text{m}$, and consists of hundreds of alternating layers of at least two substances. Based on this information, we attempted to analyze its optical transmission properties.

The transmission coefficient τ for a general k -layered structure, with $k+1$ interfaces is given by the ratio of two finite quantities as¹¹

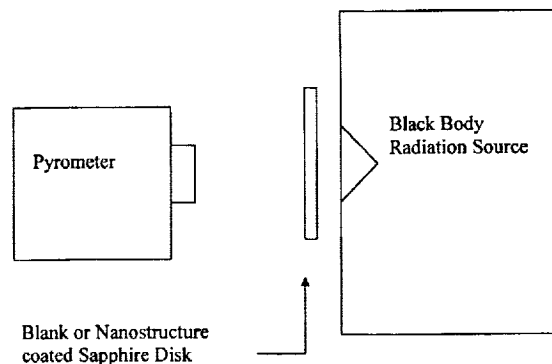


FIG. 14. Experimental arrangement to study nanostructured coating transmission.

$$\tau = \frac{t_1 t_2 t_3 \dots t_{k+1} \exp(-i[\Phi_1 + \Phi_2 + \dots + \Phi_k])}{1 + \sum r_{l_1} \cdot r_{l_2} \dots \exp(-2i[\Phi_{l_1} - \Phi_{l_2} + \dots])}, \quad (9)$$

$$\Phi_v = \phi_1 + \dots + \phi_{v-1}, \quad v = 2, 3, \dots, k+1; \Phi_1 = 0, \quad (10)$$

where t_1, t_2, \dots are the transmission coefficients at the boundary interfaces, r_1, r_2, \dots are the reflection coefficients at these interfaces, and the summation in the denominator is over all the possible even products of $r_1 r_2, \dots$. The statement "all the possible" means one must take all monotonic subsets of

$$l_1 < l_2 < \dots < l_s, \quad (11)$$

where $S = 2, 4, 6, \dots$, but never exceeding $k+1$. The quantity

$$\phi_i = 2\pi \frac{2d_i}{n_i} \frac{1}{\lambda} \quad (12)$$

is the phase difference experienced by radiation of wavelength λ passing through a layer, n_i is the nanostructured layer's refractive index, and d_i is the thickness of the nanostructured layer. For $k=1$, the case of a single layer, we have the familiar transmission formula¹²

$$\tau = \frac{t_1 t_2 \exp(-i\phi)}{1 + r_1 r_2 \exp(-2i\phi)} \quad (13)$$

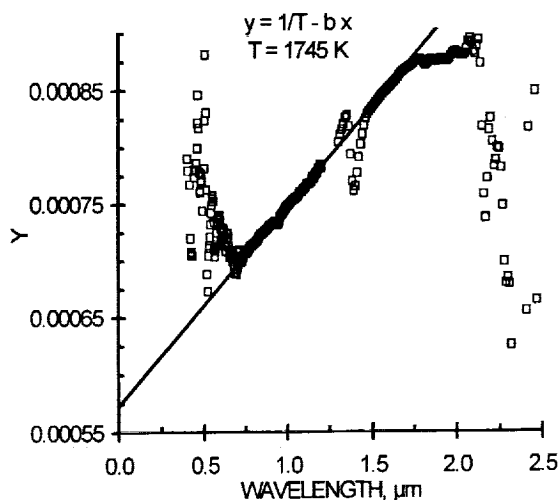


FIG. 13. Plot of the transformed radiation spectrum from a BeO gas temperature probe at 1745 K.

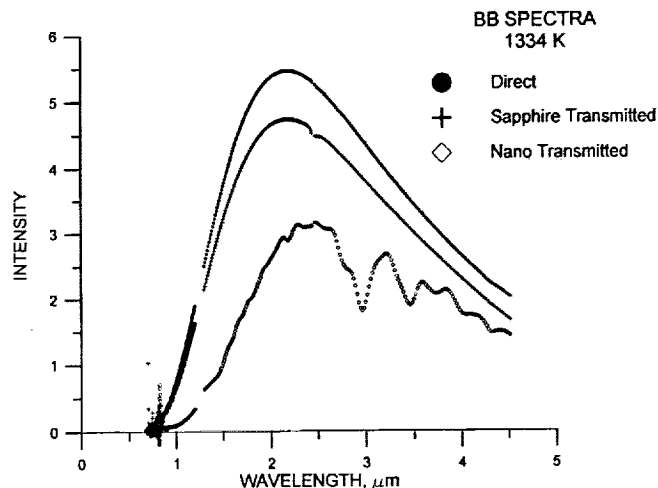


FIG. 15. A BB spectrum, this spectrum transmitted through a sapphire substrate, and also its spectrum transmitted through a sapphire substrate coated with nanostructured material.

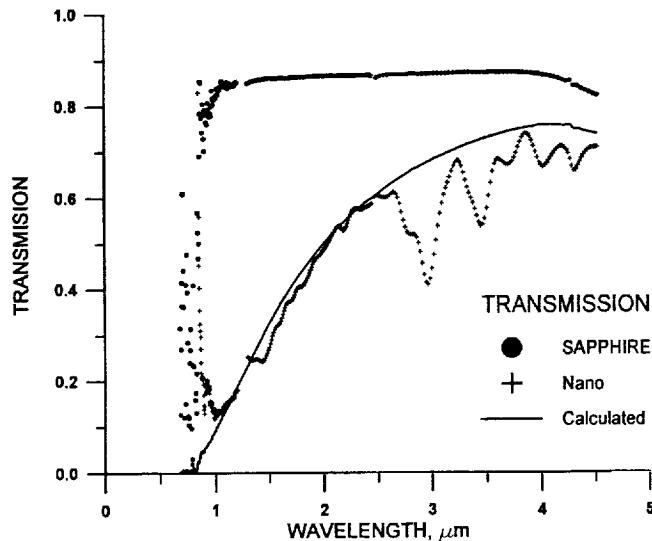


FIG. 16. Fractional transmission of BB radiation through a sapphire substrate, and through a nanostructure coated sapphire substrate.

of a single layer interference filter.

Equation (9) can be interpreted as follows: the numerator is related to the magnitude of transmitted radiation through the nanostructured layers while the denominator expresses the result of constructive and destructive interference of radiation as it passes back and forth through the many layers of the material that make up the TBC. The oscillations in the transmission curve (Fig. 16) are manifestations of this interference process. In our application, the denominator is too complicated to write down explicitly in closed form. In our analysis, it is treated as having a value of magnitude unity because the preexponential factors are all less than unity.

Assume that the nanostructure has just two different compositional layers, one of them acting as a thin separation boundary, and that the pattern is repeated. There are thus k pairs. For the i th one, t_i results from scattering through this compositional pair. In the nanostructure, the total thickness of this layer pair is d/k , where d is now the total thickness of the nanostructure layers, and k the number of pairs in them. The nanostructure is considered to be a collection of scatterers with a density of N per unit volume. Each scatterer has a scattering cross section σ . For a unit intensity, unit cross section input, the radiation that is scattered away by them is $N\sigma d/k$. The unscattered fraction will be the transmitted intensity, therefore $t_i = 1 - N\sigma d/k$. The final fraction that is transmitted after passing through k of them is $(1 - N\sigma d/k)^k$. When k is large, this becomes $\exp(-N\sigma d)$.

In the propagation of ultrasonic waves in solids, acoustic energy is attenuated due to defects according to the square of the frequency.^{13,14} If we consider the nanostructure as a collection of defects as far as optical propagation is concerned, it would be reasonable to expect that optical attenuation is similar to acoustic attenuation and would have similar frequency dependence for optical transmission, proportional to the square of the frequency, or inversely proportional to the square of the wavelength.

The transmission of sapphire was uniform throughout the investigated spectral region (Fig. 16). But the nanostruc-

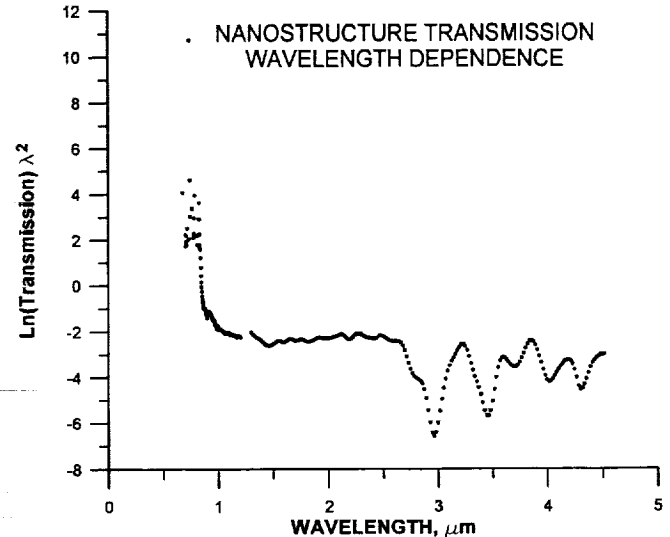


FIG. 17. Plot of the product of the logarithm of nanostructure transmission and λ^2 vs λ to show its wavelength dependence. The spike at very short wavelength is probably just noise.

ture coated sapphire transmission exhibited strong spectral variation. A plot of $\text{Ln}(\tau)\lambda^2$ vs λ is shown in Fig. 17. A constant straight line was obtained at wavelengths above 1 μm , which indicates the presence of a term inversely proportional to the square of wavelength. The peaks and valleys beyond 3 μm were due to the interference effects present in the nanostructure. From our analysis, we concluded that the wavelength dependence of nanostructured quartz substrate scattering is inverse squared in nature and is expressed by

$$\tau_{\text{nano}}(\lambda) = \tau_{\text{sap}}(\lambda) \exp\left(-Nd \frac{\alpha}{\lambda^2}\right), \quad (14)$$

where $\tau_{\text{sap}}(\lambda)$ is the transmission of the sapphire on which the nanostructure is deposited, and α is some constant. This functional spectral dependence of nanostructure transmissivity is useful and important to know when one measures the temperature of a substrate situated beneath a coating of nanostructured substance.

F. Temperature distribution measurement

High spatial resolution is necessary to measure the temperature of surfaces whose temperature varies greatly from point to point. The multiwavelength pyrometer meets this requirement by operating with a very narrow FOV of 1 mR or smaller, acquiring and processing the signal emitted from just a small region. Alternatively, there are occasions when it is desirable to determine the temperature distribution of an extensive surface by performing just one measurement. The multiwavelength pyrometer can do so when it is configured to function as a remote sensing device, operating with a very wide field of view. When the multiwavelength pyrometer is operated in this mode, its output signal represents its response to the aggregate radiation of a large nonuniform temperature surface whose elemental surfaces $da(T)$ are each at a different temperature T . The radiation spectrum at each wavelength is given by

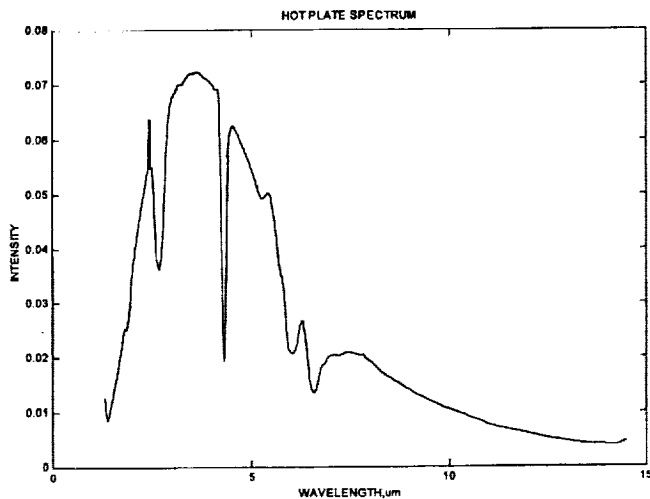


FIG. 18. Radiation spectrum of a large metal plate surface heated by a propane torch.

$$L_\lambda = \frac{c_1}{\lambda^5} \int \frac{1}{\exp(c_2/\lambda T) - 1} d(\epsilon_\lambda a(T)) \quad (15)$$

which is an integral equation. Measurement of a single radiation spectrum spanning a very wide spectral region provided the data to solve this integral equation to determine the unknown area temperature distribution $a(T)$.

Such a spectrum (Fig. 18), that of a 20 cm diameter metal plate (Fig. 19) was obtained using the multiwavelength pyrometer. The plate was raised in temperature by impinging a narrowly penciled propane torch flame at the surface that was not facing the pyrometer. The flame geometry produced a nonuniform temperature distribution on the metal plate. The pyrometer was calibrated with a black body furnace and then used to acquire the very broad spectrum of this spatially large nonuniformly heated radiating metal plate. The spectrometer's normal field of view is variable from 1 to 6 mR and is capable of operating in the spectral region between 1.3 and 14.5 μm . A modification to the spectrometer enabled it to view a much wider (6°) field. The metal plate was completely contained inside the radiometer's increased, broader field of view by varying the distance between it and the spectral radiometer.



FIG. 19. Picture of a metal plate heated by a propane torch from its back surface.

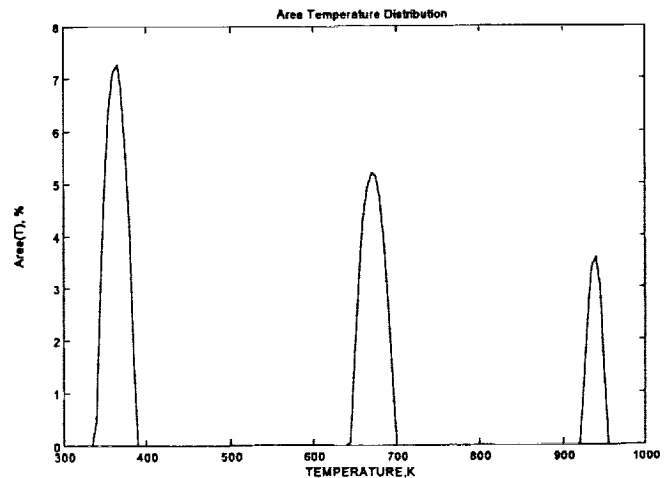


FIG. 20. Temperature distribution of the heated metal plate.

To show how Eq. (15) is solved to obtain $a(T)$, we subdivide the temperature region of interest, $T = T_0 - T_m$, into m equal intervals denoted by $T_j = T_0 + j\Delta T$, where $\Delta T = (T_m - T_0)/m$, and $j = 0$ to m is the dummy index. A piecewise integration of Eq. (15) results in

$$L_{\lambda_i} = \sum \frac{c_1}{\lambda_i^5} \frac{1}{\exp(c_2/\lambda_i T_j) - 1} \epsilon_{\lambda_i} a(T_j) \quad (16)$$

discretizing the integral equation into the matrix equation Eq. (16). The quantity on the left is an n dimensional column vector L connecting the experimental spectrum L_λ , (consisting of $n = 455$ wavelength channels of spectral data in the spectrum of Fig. 18) to the desired solution function \mathbf{a} , (an m dimensional column vector, whose elements are $a(T_j)$ in the temperature intervals $j = 1 - m$), and an $n \times m$ dimensional matrix \mathbf{K} , whose elements K_{ij} are

$$K_{ij} = \frac{c_1}{\lambda_i^5} \frac{1}{\exp(c_2/\lambda_i T_j) - 1} \quad (17)$$

It is convenient to write Eq. (16) in matrix form

$$\mathbf{L} = \mathbf{K} \cdot \mathbf{a} \quad (18)$$

Solving this matrix equation to obtain \mathbf{a} belongs to a class of "ill-posed" mathematical problems, requiring "regularization"¹⁵ to determine its solution according to

$$\mathbf{a} = (\mathbf{K}'\mathbf{K} + \alpha\mathbf{I})^{-1} \cdot (\mathbf{K}'\mathbf{L} + \alpha\mathbf{c}), \quad (19)$$

where \mathbf{I} is the identity matrix, \mathbf{K}' is the transpose of matrix \mathbf{K} , α is a scalar constant, called the regularization parameter, chosen to reduce the noise that accompanies the possible solutions which occurs during the inversion process, and \mathbf{c} is a constant matrix. The solution for \mathbf{a} in Eq. (19) is obtained by an iteration procedure described by Ohno,¹⁶ using a commercially available mathematical tool package. The result is shown in Fig. 20.

Apparent in the solution were three distinct temperature distributions centering around 375, 680, and 930 K. The 930 K temperature agreed well with the temperature measured by the multiwavelength pyrometer when it was trained on the glowing hot spot produced by the propane torch on the metal plate. This hottest temperature region was attributed to arise

from the direct impingement of the torch flame on the backside of the plate. The intermediate temperature region, 680 K, was the result of that part of the metal plate immersed in the updraft of the hot combustion products accompanying the flame. Finally, as a result of heat conduction taking place up to the time the spectrum was recorded, the remainder of the plate temperature had risen about 75 K above ambient.

The technique just described could have an important application in measuring jet engine burner pattern factors (BPF). BPF is the circumferential and radial temperature deviation from the mean temperature at the combustor exit of a jet engine. Measuring and controlling these excursions are important in active engine control technology development to achieve increased engine efficiency and long life. BPF measurement is now laboriously provided by elaborately instrumented point sensing thermocouple arrays. The multi-wavelength pyrometer can now trivially and immediately provide some aspects of this temperature distribution information in BPF measurement.

ACKNOWLEDGMENT

The authors acknowledge the reviewer for bringing to their attention a reference which addresses the error that arises from the fact that the term $(1 - \exp(-c_2/\lambda T))$ is different from unity.

¹D. P. DeWitt and G. D. Nutter, *Theory and Practice of Radiation Thermometry* (Wiley, New York, 1988).

²G. B. Hunter, C. D. Allemand, and T. W. Eagar, *Opt. Eng.* **25**, 1222 (1986).

³M. A. Khan, C. Allemand, and T. W. Eagar, *Rev. Sci. Instrum.* **62**, 392 (1991).

⁴M. A. Khan, C. Allemand, and T. W. Eagar, *Rev. Sci. Instrum.* **62**, 403 (1991).

⁵D. Ng and W. D. Williams, *Temperature*, Vol. 6 (AIP, New York, 1992), pp. 889–893.

⁶Spectrometer Model SR5000 is manufactured by CI System, Inc., 30961 W. Agoura Road, Suite 109, Westlake Village, CA 901361-4618. Spectrometer specifications are listed below. Optics: 5 in. diameter entrance aperture, reflective telescope; spectral range: 0.4–14.5 μm with various circular variable filters (CVFs); field of view: 6 mrad standard, motorized 0.3–6 mrad, wide field of view, 5.7°; spectral resolution: 1.35%–2.2% of wavelength at 3 mrad or smaller FOV using standard CVF (varies according to wavelength region); scan rates: 0.015–2 scans/s; aiming and focusing: reflex sight with focus lock; focusing range: 3 m to infinity; detector types: interchangeable, thermoelectrically or LN_2 cooled; internal black body: ambient with minimum drift and gradient; chopping frequency range: 100–1800 Hz; dynamic range: 1:500 000 and larger depending on detector; analog/digital 14 bit; noise performance: maximum 5 mdeg NET with CVF at 5 μm , InSb detector 1 Hz electronic bandwidth, 100 °C black body cavity, and filled 6 mrad FOV. This is equivalent to an NET = 8×10^{-13} W/cm²; saturation radiation: dependent upon detector; for InSb without filter, typically 5.4 μW on the detector or an equivalent radiance of a 1000 °C blackbody with 0.095 in. aperture diameter (2.4 mm) at 3 m distance. We provide this information strictly for identification purpose only.

⁷Y. A. Levendis, K. R. Estrada, and H. C. Hotel, *Rev. Sci. Instrum.* **63**, 3608 (1992).

⁸D. Ng, *Temperature Measurement of Ceramic Material* (NASA TM 1999-208850).

⁹T. J. Quinn, *Temperature* (Academic, New York, 1983), p. 361.

¹⁰G. Fralick and D. Ng, *Pyrometric Gas and Surface Temperature Measurements* (NASA TM 1999-209059).

¹¹Knittl Zdenek, *Optics of Thin Films* (Wiley, New York, 1976), pp. 47–51.

¹²Bruno Rossi, *Optics, Principle of Physics Series* (Addison-Wesley, Reading, MA, 1957), Chap. 3.

¹³H. J. Maris, *Phys. Rev.* **175**, 1077 (1966).

¹⁴T. O. Woodruff and H. Ehrenreich, *Phys. Rev.* **123**, 1553 (1961).

¹⁵I. J. D. Craig, and J. C. Brown, *Inverse Problems in Astronomy* (Hilger, Bristol, 1986).

¹⁶J. Ohno, *Temperature*, Vol. 5 (American Institute of Physics, New York, 1982), pp. 401–407.

